AIAA JOURNAL
Vol. 41, No. 12, December 2003

Identification and Control of Taylor–Görtler Vortices in Turbulent Curved Channel Flow

Chun-Xiao Xu,* Jung-Il Choi,† and Hyung Jin Sung‡
Korea Advanced Institute of Science and Technology, Daejeon 305-701, Republic of Korea

Direct numerical simulations of turbulent flows in a curved channel are performed. The drifting Taylor–Görtler vortices are identified by applying a conditional averaging. A new algorithm is proposed for identifying the drifting Taylor–Görtler vortices based on the wavelet transform of wall information. A continuous wavelet transform with Marr wavelets is employed to decompose the flow signals at a chosen length scale. An active cancellation is applied to attenuate the Taylor–Görtler vortices and to reduce the wall skin friction.

Nomenclature

H	=	channel half-width, $(R_o - R_i)/2$
l	=	wavelet scale
R	=	radius of the channel center, $(R_i + R_o)/2$
R_i	=	radius of the inner cylinder
R_o	=	radius of the outer cylinder
Re_m	=	Reynolds number, $U_m H/\nu$
Re_τ	=	Reynolds number, $u_\tau H/\nu$
r	=	radial direction in cylindrical coordinates
t	=	time
U_m	=	bulk mean velocity
u, v, w	=	velocity components in the x, y, z directions, respectively
u_τ	=	wall friction velocity
v_w	=	blowing/suction velocity at the wall
w_w	=	sliding velocity of the wall
x, y, z	=	spatial coordinates in the streamwise, wall-normal, and spanwise directions, respectively
ϵ	=	curvature parameter, H/R
θ	=	azimuthal direction in cylindrical coordinates
ν	=	kinematic viscosity
τ	=	wall shear stress

Subscripts

c	=	control
g	=	global varible
i	=	convex wall
no	=	no control
o	=	concave wall
rms	=	root mean square

Superscripts

$+$	=	wall unit
$-$	=	average in x, z, and t
$\sim$	=	average in x and t
$'$	=	total turbulence
$''$	=	underlying turbulence

Received 24 January 2003; revision received 16 June 2003; accepted for publication 30 June 2003. Copyright © 2003 by the American Institute of Aeronautics and Astronautics, Inc. All rights reserved. Copies of this paper may be made for personal or internal use, on condition that the copier pay the $10.00 per-copy fee to the Copyright Clearance Center, Inc., 222 Rosewood Drive, Danvers, MA 01923; include the code 0001-1452/03 $10.00 in correspondence with the CCC.

*Associate Professor, Department of Mechanical Engineering; currently Associate Professor, Department of Engineering Mechanics, Tsinghua University, Beijing 100084, People's Republic of China.

†Postdoctoral Student, Department of Mechanical Engineering, 373-1, Guseong-dong, Yuseong-gu.

‡Professor, Department of Mechanical Engineering, 373-1, Guseong-dong, Yuseong-gu; hjsung@kaist.ac.kr. Member AIAA.

I. Introduction

TURBULENT flow with streamline curvature is of considerable engineering interest. Taylor–Görtler vortices are the characteristic flow structures closely related with concave streamline curvature.[1] Although the geometry of a concave wall is not very complex, the boundary layer that develops on its surface is difficult to model because of the presence of streamwise Taylor–Görtler vortices.[2] The presence of the Taylor–Görtler vortices makes the flow on a concave wall three-dimensional rather than two-dimensional. As pointed out by Bradshaw,[3] the effect of any extra rate of strain imposed by streamline curvature is often an order of magnitude more important than the explicit effects of the extra terms that appear in the equations of motion.

Taylor–Görtler vortices were first studied as a kind of flow-stability problem.[4] The boundary-layer instabilities induced by wall curvature were reviewed by Saric.[5] A literature survey reveals that many experimental and numerical studies have been made on the Taylor–Görtler vortices in turbulent flows over concave surfaces.[6] The Taylor–Görtler vortices are very important in the establishment of the asymmetry between the concave and convex walls in the curved channel. Moser and Moin[7] found that Taylor–Görtler vortices make a significant contribution to the concave-side Reynolds stress, but they contribute negligibly to the convex side. The induced upwash and downwash motions serve as effective agents to transport streamwise momentum normal to the wall, thereby increasing the skin friction. The secondary flow induced by wall curvature is then very closely related with the generation of skin-friction drag.[2]

A perusal of the relevant literature discloses that the evidence for the existence of Taylor–Görtler vortices in concave-wall boundary layers is not conclusive.[1,6] The upstream flow history can exert a significant influence on the initial development of secondary flow structures in concave turbulent boundary layers.[2] Many researchers have observed a repeatable stationary pattern of spanwise variations.[3] In an attempt to impose a more regular pattern of variations, Hoffmann et al.[8] placed regularly spaced vortex generators upstream of concave surface. The resulting weak longitudinal vortices in the upstream boundary layer were amplified by the curvature, serving to "lock in" the positions of the turbulent Taylor–Görtler cells. On the other hand, Jeans and Johnston[11] did not observe the stationary pattern of roll cells in their flow-visualization study. This is presumably attributed to a lack of persistent upstream disturbances. Large-scale roll-like structures seemed to be distributed randomly in space and time over the concave wall, and they did not produce significant spanwise variations in time-averaged quantities. By using the temporal average with a finite time, Moser and Moin[7] differentiated turbulent Taylor–Görtler vortices from the underlying turbulence in a concave wall. The vortices that survive this averaging might

actually be moving or evolving on a timescale of the averaging time. Because the drifting Taylor–Görtler vortices are present, a conditional averaging technique is needed to identify the drifting vortices.

In the present study a new algorithm is developed to identify the drifting Taylor–Görtler vortices. This is based on the wavelet transform of the wall information such as the velocity gradient at the wall. A continuous wavelet transform with Marr wavelets is employed to decompose the flow signals at a chosen length scale. The scale is determined by considering the instability theory that the width of the wavelet is equivalent to the wavelength of the Taylor–Görtler vortices.[4] The active cancellation is applied to attenuate the large-scale Taylor–Görtler vortices and attendant small-scale vortices near the wall.[10] The cancellation is made based on the input velocity at the wall, which is proportional and opposite to the instantaneous velocity at a location near the wall. Several active cancellations are tested to assess the effectiveness of the controls. It is found that a combined active cancellation at the concave wall makes the Taylor–Görtler vortices break up to smaller vortices and weaken their strengths and contributions to Reynolds stress.

II. Direct Numerical Simulation

Direct numerical simulations of turbulent curved channel flow are performed. Figure 1 shows a schematic diagram of the flow domain and the coordinate system. The flow domain is a sector between two concentric cylinders. We use r, θ, and z to denote the radial, azimuthal, and spanwise directions, respectively. As shown in Fig. 1, $R = (R_i + R_o)/2$ is the mean radius and $H = (R_o - R_i)/2$ is the half channel width. The ratio $\epsilon = H/R$ is defined as the curvature parameter.

The three-dimensional time-dependent incompressible Navier–Stokes equations are solved by a spectral method.[11] To employ Chebyshev polynomials and Fourier series, the (r, θ, z) coordinates are transformed into (x, y, z) coordinates by $x = -R\theta/H$, $y = (r - R)/H$, and $z = z/H$. The flow is driven by the mean pressure gradient in the x direction.

To solve the governing equations, a Chebyshev-collocation method is used in the wall-normal direction, and a dealiased Fourier–Galerkin method is adopted in the streamwise and spanwise directions for the spatial discretization. A third-order time-splitting method is employed to carry out the time advancement.[11] A total time step is divided into three substeps, which in turn solve the nonlinear terms, the pressure terms, and the viscous terms. The pressure is obtained by solving the pressure Poisson equation. Periodic boundary conditions are used in the streamwise and spanwise directions, and no-slip conditions are applied at the walls. All of the simulations are performed with constant streamwise mass flux. The control to the flow through blowing and suction or sliding at the wall is realized by direct consideration of the wall boundary conditions.[10] The Reynolds number is $Re_m = 2.6 \times 10^3$ based on the bulk velocity U_m and channel half-width H. The curvature parameter is chosen at $\epsilon = 0.0127$. The domain extends to $4\pi H \times 2H \times 8\pi H/3$ in the streamwise, wall-normal, and spanwise directions, in concert with a grid size of $64 \times 64 \times 128$. For the validation of the domain size, the correlation functions are compared with those of Moser and Moin.[7] In wall units the effective grid spacing is $\Delta x_c^+ = R^+ \Delta\theta = 36$ in the streamwise direction and $\Delta z^+ = 12$ in the spanwise direction. In the radial direction, the closest effective grid point to the wall is $\Delta y^+_{\max} = 8.2$. A time step of $\Delta t = 0.01 H/U_m$ is used in the present simulation.

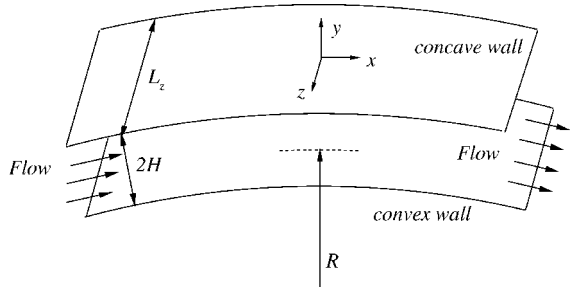

Fig. 1 Flow geometry and coordinate system.

In general, Taylor–Görtler vortices (TGVs) can be made stationary by introducing artificial disturbances upstream of the curved section.[7] In the present computation, however, the TGVs themselves act as the analogous upstream disturbances by using the periodic boundary conditions in the streamwise direction. Nothing can preclude them from moving in the spanwise direction. Accordingly, the strength and effect of the TGVs are underestimated by conventional temporal average. To avoid the underestimation, two types of averaging are employed in the present study. Suppose q is a flow quantity, we use $\bar{q} = \langle q \rangle_{x,z,t}$ to denote the average in x, z, and t, and $\tilde{q} = \langle q \rangle_{x,t}$ to denote the average in just x and t. Hence, $\tilde{q} - \bar{q}$ describes a state of the Taylor–Görtler vortices. The fluctuations of q with respect to $\bar{q}$ are defined as $q' = q - \bar{q}$ and referred to as total turbulence, whereas the fluctuations with respect to $\tilde{q}$ are defined as $q'' = q - \tilde{q}$ and referred to as underlying turbulence. It is obvious that $q' - q'' = \tilde{q} - \bar{q}$.

Because of the asymmetry of the curved channel with respect to the channel centerline, the wall values at the convex and concave walls are different.[7] The shear stress at the convex wall (inner wall) is

$$\tau_i = \left(\frac{1}{Re} \frac{\mathrm{d}\bar{u}}{\mathrm{d}y} \right)_{y=-1} \tag{1}$$

whereas the shear stress at the concave wall (outer wall) is

$$\tau_o = \left(\frac{1}{Re} \frac{\mathrm{d}\bar{u}}{\mathrm{d}y} \right)_{y=1} \tag{2}$$

The mean streamwise pressure gradient to maintain a constant mass flux can be determined by

$$\frac{\partial \bar{p}}{\partial x} = \frac{(1-\epsilon)^2 \tau_i + (1+\epsilon)^2 \tau_o}{2} \tag{3}$$

Accordingly, three different wall friction velocities can be defined as

$$u_{\tau i} = \sqrt{\frac{\tau_i}{\rho}}, \qquad u_{\tau o} = \sqrt{\frac{\tau_o}{\rho}}, \qquad u_{\tau g} = \sqrt{\frac{1}{\rho}\frac{\partial \bar{p}}{\partial x}} \tag{4}$$

III. Identification of the Taylor–Görtler Vortices

Before describing the identification method used in the present study, we first explain the location of the drifting TGVs. As mentioned earlier, the TGVs are large streamwise counter-rotating cells. Between the vortices the flow away from the concave wall is relatively stronger than the flow towards the concave wall. At the boundaries between the vortices where the fluids move away from the concave wall, the boundary-layer thickness is greatest, and the skin friction is lowest.[7] The streamwise averaged (v, w) vectors along with the spanwise variation of the streamwise averaged wall shear stress at three different time instants are displayed in Fig. 2. At $t = 1050$ the drifting TGVs are located at about $z = 3.0$, then they move to $z = 2.2$ at $t = 1250$ and to $z = 1.4$ at $t = 1450$. Compared with the corresponding vector plots, the spanwise variations of the concave wall shear stress take local minimum values at the locations of the TGVs. However, the local minimum points of $\partial u/\partial y|_{y=1}$ are not always equivalent to the locations of the TGVs. This is because the wall information is directly influenced by the near-wall small-scale structures. Usually the wavelength of the TGVs is of the order of channel width, which is much larger than the turbulent coherent structures.[4] A multiscale decomposition by the wavelet analysis can help us to distinguish the points of the TGVs from the streamwise vortices.

In the present study a continuous wavelet transform with Marr wavelets is employed to decompose the flow signals at a chosen scale.[12] The mother function of the Marr wavelets is

$$\psi(z) = (1 - z^2) e^{-z^2/2} \tag{5}$$

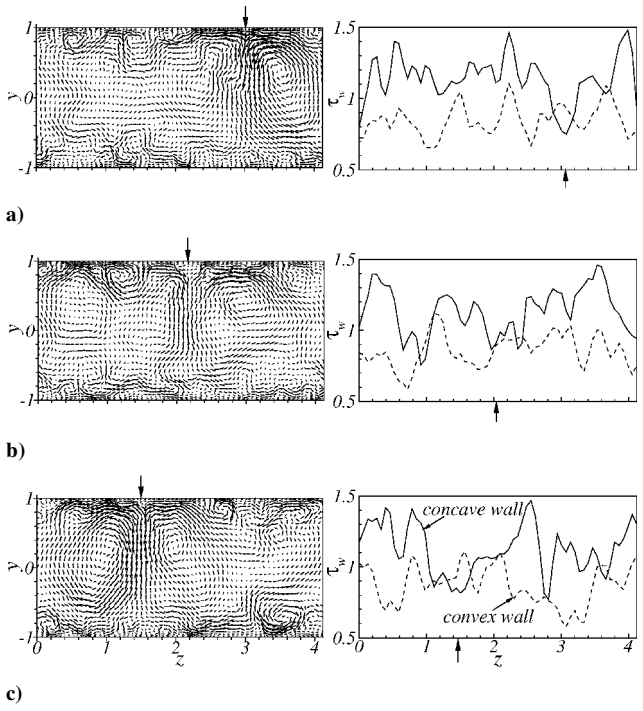

Fig. 2 (v, w) vectors and wall shear stress: a) $t = 1050$, b) $t = 1250$, and c) $t = 1450$.

The wavelets can be constructed from the mother function by dilation and translation as

$$\psi_{lz'}(z) = l^{-\frac{1}{2}}\psi[(z - z')/l] \tag{6}$$

where l and z' are the scale and position parameters, representing the dilation and translation of the wavelets, respectively. The continuous wavelet transform of a function $f(z)$ is

$$\tilde{f}(l, z') = \int_{-\infty}^{+\infty} f(z)\psi^*_{lz'}(z)\,\mathrm{d}z = \int_{-\infty}^{+\infty} \hat{f}(k)\hat{\psi}^*_{lz'}(k)\,\mathrm{d}k \tag{7}$$

The wavelet scale l is chosen at which the width of the wavelet is approximately equivalent to the wavelength of the TGVs. This is based on the instability theory that the maximum amplification wavelength is estimated from the maximum energy spectra of the wavelet coefficients.[4] In the present study ($\epsilon = 0.0127$) the wavelet scale is chosen at $l = 0.75$, where the wavelength of the TGVs is approximately $4H$.

Because the vortices are counter-rotating between the TGVs, the spanwise velocity w goes to zero near the wall. Hence, we can use the zero crossing of $\partial w/\partial y|_{y=1}$ as well as the local minimum of $\partial u/\partial y|_{y=1}$ in the spanwise variation to identify the location of the TGVs. Because the distribution of the local minimum of $\partial u/\partial y|_{y=1}$ can be greatly influenced by wall actuations,[10] the zero crossing of $\partial w/\partial y|_{y=1}$ is employed in the present study. Figure 3 shows an example of the identification by using the wavelet coefficients of $\partial w/\partial y|_{y=1}$. The dashed line in Fig. 3a shows the distribution of streamwise averaged $\partial w/\partial y|_{y=1}$ in the spanwise direction, and the solid line is its wavelet coefficient. The dashed line is very fluctuating and has many zero-crossing points. The wavelet coefficient represents a filtered signal at the chosen scale. The corresponding (v, w) vectors in the (y, z) plane are displayed in Fig. 3b. Three zero-crossing points with a positive spanwise slope are detected, which are indicated by A, B, and C, respectively. A closer inspection of the vector plots discloses that the locations of the TGVs are identified by the three points. Other three zero-crossing points with a negative spanwise slope indicate the positions between two TGVs at which the flow is directed toward the concave wall. The method of identifying the TGVs is summarized as follows:

1) Calculate the spanwise distribution of the streamwise averaged $\partial w/\partial y|_{y=1}$.

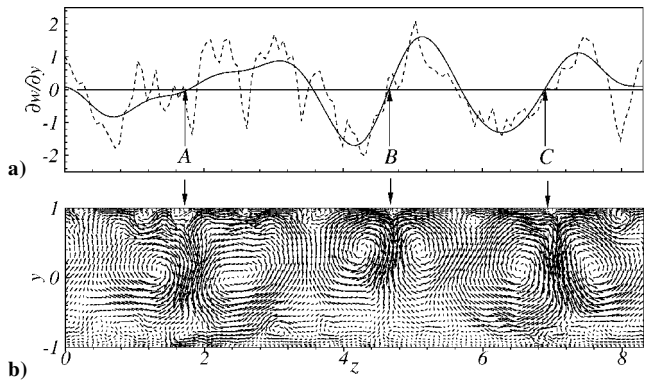

Fig. 3 Identification of the Taylor–Görtler vortices: a) $\partial w/\partial y|_w$ and its wavelet coefficients and b) (v, w) vectors.

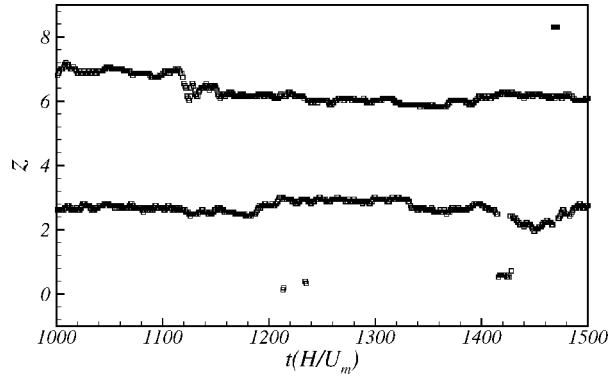

Fig. 4 Trajectory of the Taylor–Görtler vortices.

2) Apply the wavelet transform for the preceding signal at the chosen scale.

3) Choose the zero-crossing points with a positive spanwise slope of the wavelet coefficient.

Figure 4 shows the locations of the TGVs at different time instants. To set statistical properties of the TGVs, an ensemble average taken along the center positions of the TGVs is performed. The statistics are then obtained by averaging more than 1000 sample flowfields over x and t. As shown in Fig. 4, the mean wavelength of the TGVs is about $4H$ between two pairs of TGVs.

To see the contributions of TGVs, the ensemble-averaged (v, w) vectors and Reynolds stress $(u' - u'')(v' - v'')$ are displayed in Fig. 5. The spanwise variations of the wall shear stresses along both walls are also shown for comparison. A strong positive stress appears close to the concave wall ($z = 0$). This is caused by the convection of low-speed fluid away from the concave wall by a strong fluid motion in the normal direction. The concave wall shear stress reaches a minimum between the TGVs, while the convex wall shear stress has a minimum at the corresponding position.[13] In the present simulation the Reynolds numbers are $Re_{\tau i} = 153$, $Re_{\tau o} = 182$, and $Re_\tau = 170$. The maximum value of the local Reynolds stress of the TGVs is $1.19u_\tau^2$.

IV. Control of the Taylor–Görtler Vortices

As mentioned earlier, the active cancellation is applied to attenuate the TGVs and to reduce the drag. The cancellations are realized by the blowing/suction velocity at the wall v_w and the sliding velocity at the wall w_w. In the following, we use 2Dv and 2Dw to denote two-dimensional controls by the wall blowing/suction velocity v and the wall sliding velocity w at $y^+ \approx 10$, respectively. 1Dv denotes one-dimensional control in the normal velocity v at $y^+ \approx 110$. As shown in Fig. 6, the normal velocity of the TGVs is maximum at $y^+ \approx 110$, which corresponds to $y \approx 0.85$. 1Dw represents one-dimensional control in the spanwise velocity w at $y^+ \approx 26$ ($y \approx -0.4$), where the spanwise velocity of the TGVs is maximum. These one-dimensional controls aim at the attenuation of the TGVs.

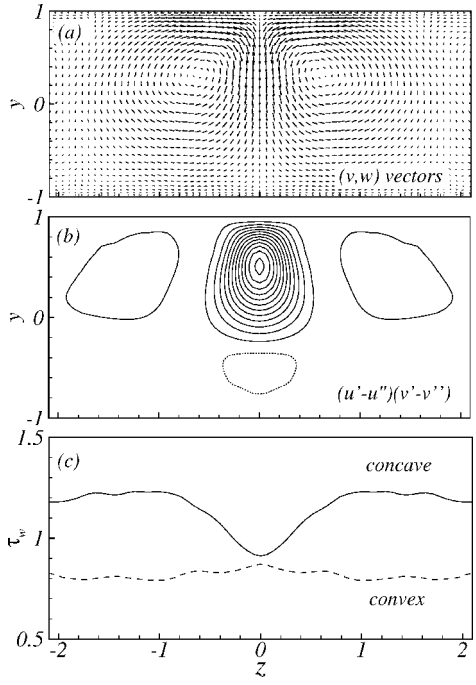

Fig. 5 a) (v, w) vectors, b) Reynolds shear stress, and c) wall shear stress.

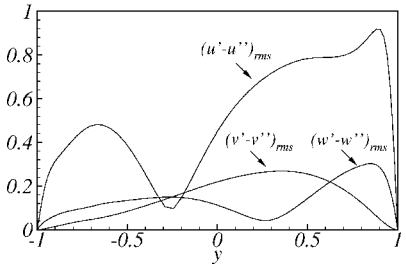

Fig. 6 Turbulence intensities contributed by Taylor–Görtler vortices.

The drag-reduction rates under eight different controls are listed in Table 1. The drag-reduction rate at each wall is measured by $(1 - \tau_c/\tau_{no}) \times 100$, where τ_{no} and τ_c are the mean shear stresses at the wall before and after control. Because the drag-reductionrates at two walls are different, a global drag-reductionrate is defined by the mean streamwise pressure gradient, $[1 - (\mathrm{d}\bar{p}/\mathrm{d}x)_c/(\mathrm{d}\bar{p}/\mathrm{d}x)_{no}] \times 100$. Here, $(\mathrm{d}\bar{p}/\mathrm{d}x)_{no}$ and $(\mathrm{d}\bar{p}/\mathrm{d}x)_c$ are the mean pressure gradients before and after control. By this definition, the constant mass-flow rate is maintained. As shown in Table 1, the local drag-reduction rates by 2Dv and 2Dw at the convex wall are larger than those at the concave wall. However, the global drag-reduction rates at the convex wall are smaller than those at the concave wall. This is because the magnitude of friction drag at the concave wall is larger than that at the convex wall. It is seen that 2Dw at the concave wall is slightly more effective than 2Dv at the concave wall. As mentioned earlier, the main goal of the control is to attenuate the TGVs by one-dimensional active cancellation. As shown in Table 1, the cancellations by 1Dv and 1Dw are effective in suppressing the TGVs. However, the local and global friction drags at the wall are not reduced, even increased. In particular, 1Dv gives a significant increase of drag, while 1Dw is weak. Although the TGVs are suppressed by 1Dv, the friction drag near the wall is then increased by the high momentum actuation by 1Dv. To achieve the suppression of the TGVs as well as the drag reduction at the wall, a combined control is proposed in the present study. As shown in Table 1, an optimum choice is 1Dw + 2Dv at the concave wall. This gives a global drag reduction by 11.9% and a local drag reduction by 20.4%, respectively.

Table 1 Drag-reduction rates, %

Case	Acting wall	$\left[1 - \frac{(\mathrm{d}\bar{p}/\mathrm{d}x)_c}{(\mathrm{d}\bar{p}/\mathrm{d}x)_{no}}\right] \times 100$	$\left[1 - \frac{\tau_c}{\tau_{no}}\right] \times 100$
2Dv	Convex	12.4	31.3
2Dw	Convex	12.2	28.6
2Dv	Concave	13.1	21.0
2Dw	Concave	14.5	23.2
1Dv	Concave	−19.6	−26.9
1Dw	Concave	−1.3	−0.9
1Dw + 2Dv	Concave	11.9	20.4
1Dw + 2Dw	Concave	7.9	14.4

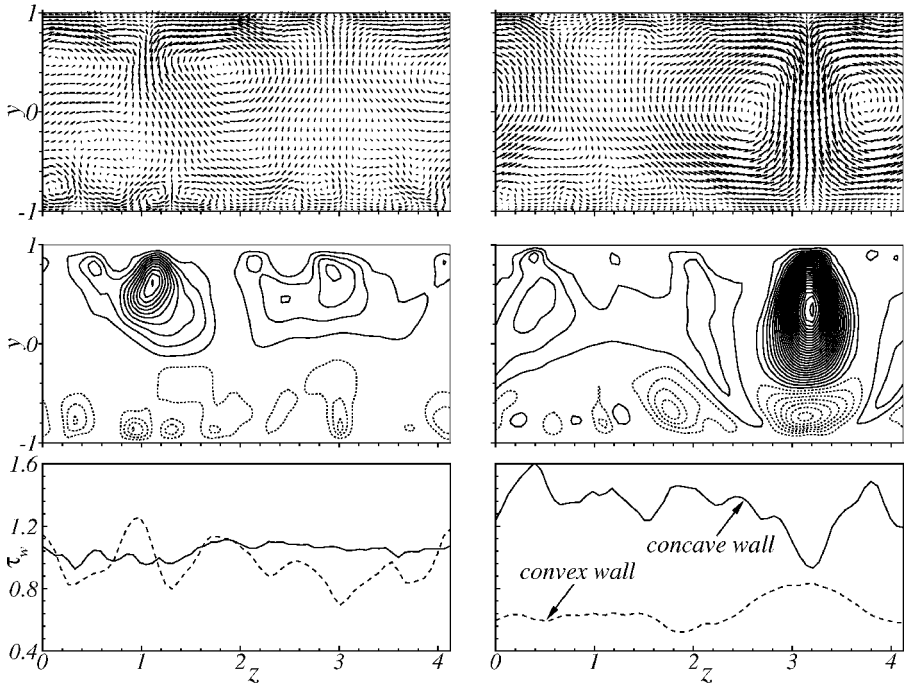

a) 2Dv at concave wall **b) 2Dv at convex wall**

Fig. 7 The (v, w) vectors, Reynolds stress, and wall shear stress by 2Dv: a) concave wall and b) convex wall.

To see the influences of eight different controls on the TGVs, (u, w) vectors, Reynolds stresses, and wall shear stresses are displayed in Figs. 7–10. These are obtained by the aforestated ensemble averaging in the streamwise direction and in time. For 2Dv at the concave wall in Fig. 7a, the TGVs are weakened, and the corresponding Reynolds stress is also attenuated. The shear stress at the concave wall is reduced similar to the level at the convex wall. There is no sharp local minimum in the spanwise variation of wall shear stress between the TGVs. Figure 7b shows the results of 2Dv at the convex wall. The TGVs are strengthened and shifted closer to the convex wall. The Reynolds stress is also intensified. Not only the local minimum in the spanwise variation of the concave wall shear stress, but also the local maximum in the spanwise variation of the convex wall shear stress are found, indicating that the blowing and suction at the convex wall act as an increase of the curvature in the preceding section. Figure 8 shows the results of 2Dw. The sliding velocity w either at the concave wall or at the convex wall cannot effectively give an influence on the strength and the position of the TGVs. The results of 1Dv and 1Dw at the concave wall are shown in Fig. 9. The TGVs disappear completely under 1Dv, as shown in Fig. 9a. This is because an active cancellation is effectively performed at $y^+ \simeq 110$ by the actuating velocities. For 1Dw, the TGVs are also greatly suppressed in Fig. 9b. As mentioned earlier, 1Dw is effective in suppressing the TGVs, and 2Dv and 2Dw are effective in reducing the wall friction. The combined controls on the TGVs are displayed in Fig. 10. It is seen that 1Dw + 2Dv at the concave wall is similar to 1Dw + 2Dw at the concave wall. They both make the TGVs break up to smaller vortices, and weaken their strengths and contributions to Reynolds stress.

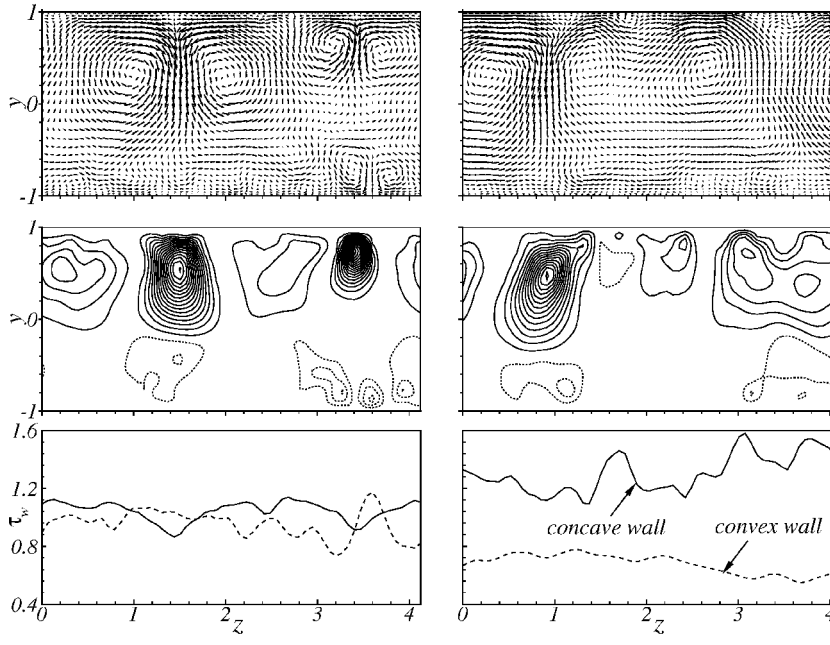

a) 2Dw at concave wall b) 2Dw at convex wall

Fig. 8 The (v, w) vectors, Reynolds stress, and wall shear stress by 2Dw: a) concave wall and b) convex wall.

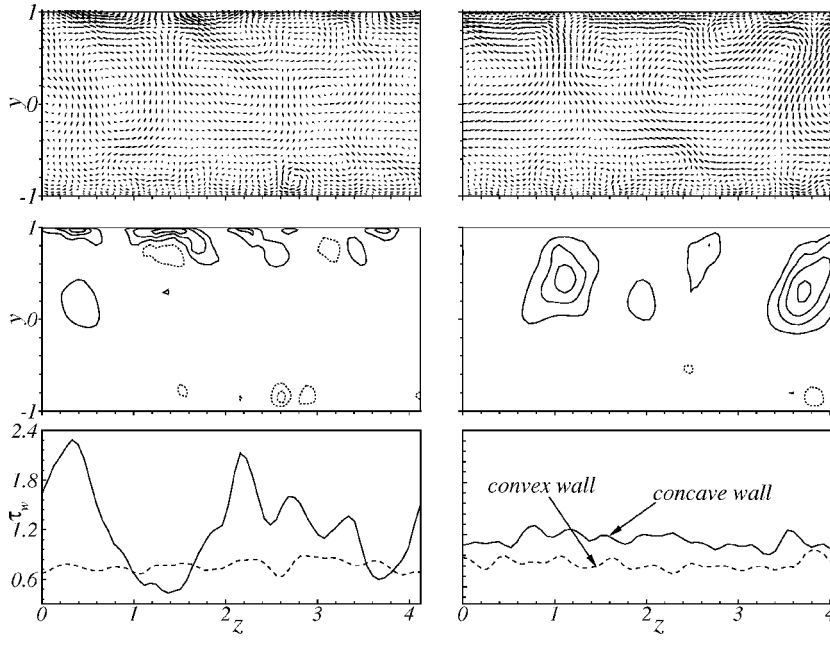

a) 1Dw at concave wall b) 1Dw at convex wall

Fig. 9 The (v, w) vectors, Reynolds stress, and wall shear stress: a) 1Dv and b) 1Dw.

In the present curved channel flow the mean wall friction can be decomposed into three parts; laminar, TGV, and turbulence, respectively. The laminar part is the viscous shear stress of laminar flow at the same mass flux, and it is irreducible by the flow manipulation. In turbulent flow the Reynolds stress $\overline{u'v'}$ can be decomposed into

$$\overline{u'v'} = \overline{(\tilde{u} - \bar{u})(\tilde{v} - \bar{v})} + \overline{u''v''} \tag{8}$$

where $\overline{(\tilde{u} - \bar{u})(\tilde{v} - \bar{v})}$ represents the contribution of the TGVs and $\overline{u''v''}$ denotes the contribution of turbulence. When the active cancellations are applied at the concave wall, the contributions of three parts to the mean wall friction are summarized in Table 2. At the concave wall both turbulence and TGV are suppressed by 2Dv and 1Dw + 2Dv, compared with no control. In particular, TGV is greatly suppressed by 1Dw + 2Dv. The portion of TGV to the total wall friction is very small when 1Dw + 2Dv is applied. However, the role of TGV at the convex wall is relatively smaller than that at the concave wall. It is seen that 1Dw + 2Dv is not effective in reducing the mean wall friction at the convex wall.

The statistical contributions of the TGVs to the velocity components and Reynolds stress under 2Dv and 1Dw + 2Dv at the concave wall are displayed in Fig. 11. For comparison, the results of no control are also included. It is generally seen that 1Dw + 2Dv is most effective in suppressing the turbulent intensities and Reynolds stress. The suppression by 2Dv is also apparent. The rms of total turbulent velocity fluctuations and Reynolds stress are shown in Fig. 12 to further depict the influence of 2Dv and 1Dw + 2Dv. By the active cancellations turbulent fluctuations are suppressed near the concave wall, whereas they are enhanced at the concave wall. The profiles are less asymmetric with respect to the channel center. The asymmetric profiles indicate that the streamwise and normal fluctuations are mutually correlated on the concave side rather than on the convex side. This is attributed to the contribution of the TGVs.[7] Because of the present cancellations, the asymmetry is recovered to the symmetry. For example, the zero-crossing point in the Reynolds stress of no control is observed at $y = -0.2$ in Fig. 12d, whereas it moves to $y = -0.1$ in the cancellation.

Table 2 Contributions to mean wall friction ($\times 10^{-3} \rho U_m^2$)

Case	Laminar	TGV	Turbulence	Total
		Concave wall		
No control	1.14	0.70	3.03	4.87
2Dv	1.14	0.43	2.33	3.91
1Dw + 2Dv	1.14	0.20	2.50	3.84
		Convex wall		
No control	1.16	0.13	2.25	3.54
2Dv	1.16	0.11	2.16	3.44
1Dw + 2Dv	1.16	0.05	2.34	3.56

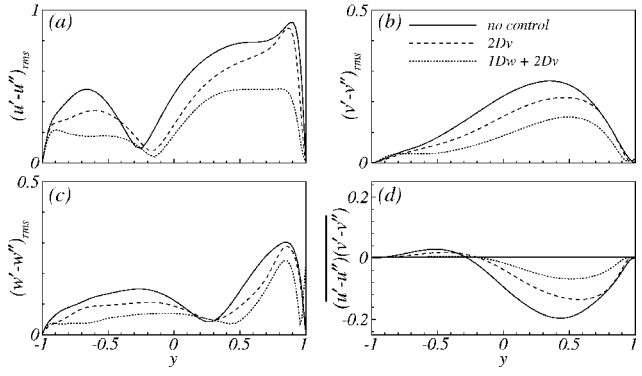

Fig. 11 Comparison of the controls: a) $(u' - u'')_{\rm rms}$, b) $(v' - v'')_{\rm rms}$, c) $(w' - w'')_{\rm rms}$, and d) $\overline{(u' - u'')(v' - v'')}$.

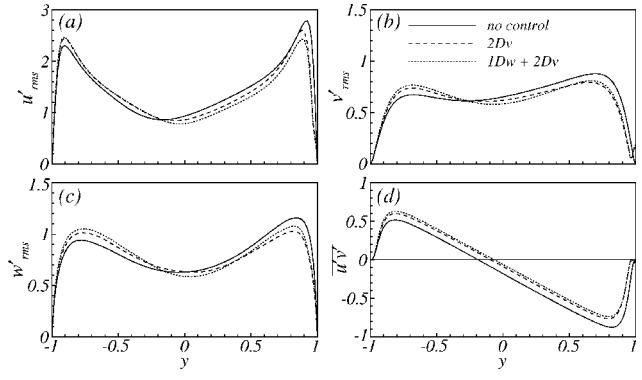

Fig. 12 Comparison of the controls: a) $u'_{\rm rms}$, b) $v'_{\rm rms}$, c) $w'_{\rm rms}$, and d) $\overline{u'v'}$.

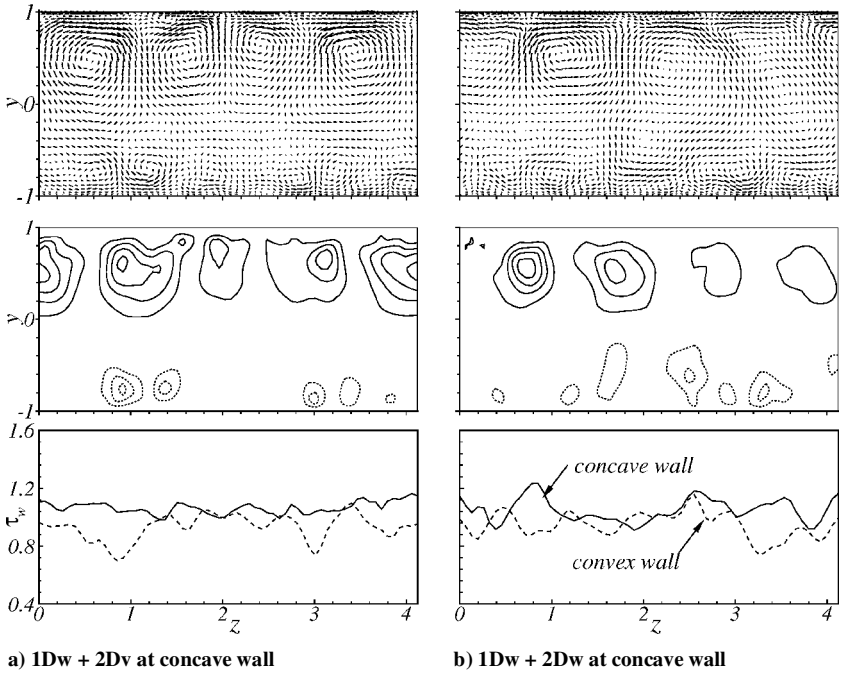

a) 1Dw + 2Dv at concave wall **b) 1Dw + 2Dw at concave wall**

Fig. 10 The (v, w) vectors, Reynolds stress, and wall shear stress: a) 1Dw + 2Dv and b) 1Dw + 2Dw.

V. Conclusions

A new algorithm has been proposed for identifying the drifting Taylor–Görtler vortices in turbulent curved channel flow. A continuous wavelet transform with Marr wavelets was employed to decompose the flow signals at a chosen length scale. The positions of the Taylor–Görtler vortices were the zero-crossing points with a positive spanwise slope of the wavelet coefficients. To suppress the Taylor–Görtler vortices near the concave wall, one-dimensional active cancellation was applied. The one-dimensional active cancellation in the wall-normal direction was effective to attenuate the Taylor–Görtler vortices. However, because of the high momentum actuation at the wall the friction drag near the wall was increased. To achieve the suppression of the Taylor–Görtler vortices as well as the wall friction reduction, a combined control was imposed at the concave wall. The drag reduction was estimated by 11.9% globally.

Acknowledgment

This work was supported by a grant from the National Research Laboratory of the Ministry of Science and Technology, Republic of Korea.

References

[1]Swearingen, J., and Blackwelder, F., "The Growth and Breakdown of Streamwise Vortices in the Presence of Wall," *Journal of Fluid Mechanics*, Vol. 182, 1987, pp. 255–290.

[2]Lund, T. S., and Moin, P., "Large-Eddy Simulation of a Concave Wall Boundary Layer," *International Journal of Heat Fluid Flow*, Vol. 17, 1996, pp. 290–295.

[3]Bradshaw, P., "Effects of Streamline Curvature on Turbulent Flow," AGARDograph 169, 1973.

[4]Görtler, H., "On the Three-Dimensional Instability of Laminar Boundary Layers on Concave Walls," NACA TM1375, 1940.

[5]Saric, W. S., "Görtler Vortices," *Annual Review of Fluid Mechanics*, Vol. 26, 1994, pp. 379–409.

[6]Patel, V. C., and Sotiropoulos, F., "Longitudinal Curvature Effects in Turbulent Boundary Layers," *Progress in Aerospace Sciences*, Vol. 33, 1997, pp. 1–70.

[7]Moser, R. D., and Moin, P., "The Effects of Curvature in Wall-Bounded Turbulent Flows," *Journal of Fluid Mechanics*, Vol. 175, 1987, pp. 479–510.

[8]Hoffmann, P. H., Muck, K. C., and Bradshaw, P., "The Effect of Concave Surface Curvature on Turbulent Boundary Layers," *Journal of Fluid Mechanics*, Vol. 161, 1985, pp. 371–403.

[9]Jeans, A. H., and Johnston, J. P., "The Effects of Concave Curvature on Turbulent Boundary Layer Structure," *IUTAM Symposium on Structure of Complex Turbulent Shear Flow*, edited by R. Dumas and L. Fulachier, Springer, New York, 1982.

[10]Choi, H., Moin, P., and Kim, J., "Active Turbulence Control for Drag Reduction in Wall-Bounded Flows," *Journal of Fluid Mechanics*, Vol. 262, 1994, pp. 75–110.

[11]Karniadakis, G. E., Israeli, M., and Orszag, S. A., "High-Order Splitting Methods for the Incompressible Navier–Stokes Equations," *Journal of Computational Physics*, Vol. 97, 1991, pp. 414–443.

[12]Farge, M., "Wavelet Transforms and Their Applications to Turbulence," *Annual Review of Fluid Mechanics*, Vol. 24, 1992, pp. 395–457.

[13]So, R. M. C., and Mellor, G. L., "Experiment on Convex Curvature Effects in Turbulent Boundary Layers," *Journal of Fluid Mechanics*, Vol. 60, 1973, pp. 43–62.

R. M. C. So
Associate Editor